Coseismic and early postseismic slip for the 2003 Tokachi-oki earthquake sequence inferred from GPS data

Shin'ichi Miyazaki[1] and Kristine M. Larson[2]

Received 10 October 2007; revised 21 December 2007; accepted 4 January 2008; published 20 February 2008.

[1] Early afterslip following the 2003 Tokachi-oki earthquake is investigated using subdaily GPS time series. Afterslip results are compared with the coseismic slip for the M8 mainshock and the M7.4 aftershock. Afterslip between those two earthquakes is inferred at the southwestern adjacent region of the mainshock, between two epicentral regions, which possibly triggered the aftershock in the southwest. Subsequently, deeper slip occurs. The afterslip loci are distinct from the rupture regions. The non-uniform propagation of afterslip may reflect the depth-dependence of the effective normal stress and the distance between the closest unstable slip patches.
Citation: Miyazaki, S., and K. M. Larson (2008), Coseismic and early postseismic slip for the 2003 Tokachi-oki earthquake sequence inferred from GPS data, *Geophys. Res. Lett.*, *35*, L04302, doi:10.1029/2007GL032309.

1. Introduction

[2] Postseismic deformation is widely observed following large earthquakes. Unlike imaging of high-speed rupture, where seismic networks provide the most important constraints, postseismic deformation is best recorded by geodetic networks. Although traditional terrestrial geodetic instruments such as tiltmeters and strainmeters can detect postseismic deformation [*Kawasaki et al.*,1995], they suffer from temporally correlated noise which is associated with, for example, rainfall, making it difficult to identify the signal for periods longer than a few days. The deployment of dense arrays of continuous GPS receivers in plate boundary zones has largely solved this difficulty by providing stable measurements. Postseismic deformation over several years is now clearly detected with great precision [e.g. *Heki et al.*, 1997].

[3] Large GPS networks can also be used to constrain slip during large earthquakes, either from a geodetic inversion [*Freymueller et al.*, 1994; *Johnson et al.*, 2001] or a combined seismic-geodetic inversion [*Ji et al.*, 2004; *Ma et al.*, 2001]. For both postseismic studies and rupture inversions, daily GPS time series are traditionally used. In this type of GPS data analysis, one assumes that the GPS stations did not move during the 24 hours following the earthquake. This analysis strategy suppresses subdaily noise in the GPS phase data and results in precisions from a few mm (horizontal) to 6–10 mm (vertical). On the other hand, this strategy makes it impossible to completely separate coseismic effects and early postseismic deformation. Using GPS measurements to estimate subdaily positions should be able to help us resolve which slip occurred coseismically and postseismically, providing greater insight for studies of slip propagation and stress transfer.

[4] In this study, subdaily GPS positions are estimated for the 2003 Tokachi-oki earthquake sequence. The GPS time series are then inverted to infer the space-time afterslip evolution. These are compared with coseismic slip distributions for the mainshock and its largest aftershock. Finally, we compare those slip distributions and discuss the frictional properties on the plate interface.

2. Tokachi-oki Earthquake

[5] The 2003 September 25 (19:50 UTC) Tokachi-oki earthquake (M $\sim$ 8) was the first megathrust earthquake in Japan recorded by its nationwide GPS network, GEONET, since its densification (Figure 1). It was followed by a M7.4 aftershock at 21:08 UTC on the same day. Slip distributions for the mainshock derived from 24-hour averaged GPS positions have been previously presented [*Miura et al.*, 2004; *Koketsu et al.*, 2004; *Ozawa et al.*, 2004]. *Miura et al.* [2004] and *Koketsu et al.* [2004] found the maximum slip $\sim$30 km north to NNW of its epicenter while *Ozawa et al.* [2004] inferred the peak slip $\sim$50 km NW of the epicenter. All of those studies located the maximum slip to be deeper than the hypocenter. There were also several seismic analyses of the earthquake rupture [*Yamanaka and Kikuchi*, 2003; *Yagi*, 2004; *Honda et al.*, 2004; *Koketsu et al.*, 2004; *Miyazaki et al.*, 2004b]. The cumulative slip distributions predicted for these seismic studies vary significantly.

[6] The space-time evolution of afterslip in the months following the Tokachi-oki earthquake has also been previously studied [*Miyazaki et al.*, 2004a; *Ozawa et al.*, 2004]. Afterslip is generally distributed around the rupture region, and cannot be fit by viscoelastic rebound [*Tanaka*, 2007]. Both of these postseismic studies focused on data collected more than one day after the mainshock. *Miyazaki et al.* [2004a] used daily GPS time series and did not model afterslip on September 25th or 26th. *Ozawa et al.* [2004] also used daily GPS time series to model the "coseismic" slip for the mainshock and the afterslip from September 26 to March 6, 2004. However daily GPS positions for September 25 included steps associated with the mainshock, the M7.4 aftershock, and the early phase of afterslip, and hence the inferred "coseismic" slip may not be accurate.

3. GPS Data and Inversion

[7] Although *Miyazaki et al.* [2004b] showed that GPS data sampled at 1-Hz can be used to estimate slip for the

[1]Earthquake Research Institute, University of Tokyo, Tokyo, Japan.
[2]Department of Aerospace Engineering Sciences, University of Colorado, Boulder, Colorado, USA.

0094-8276/08/2007GL032309$05.00

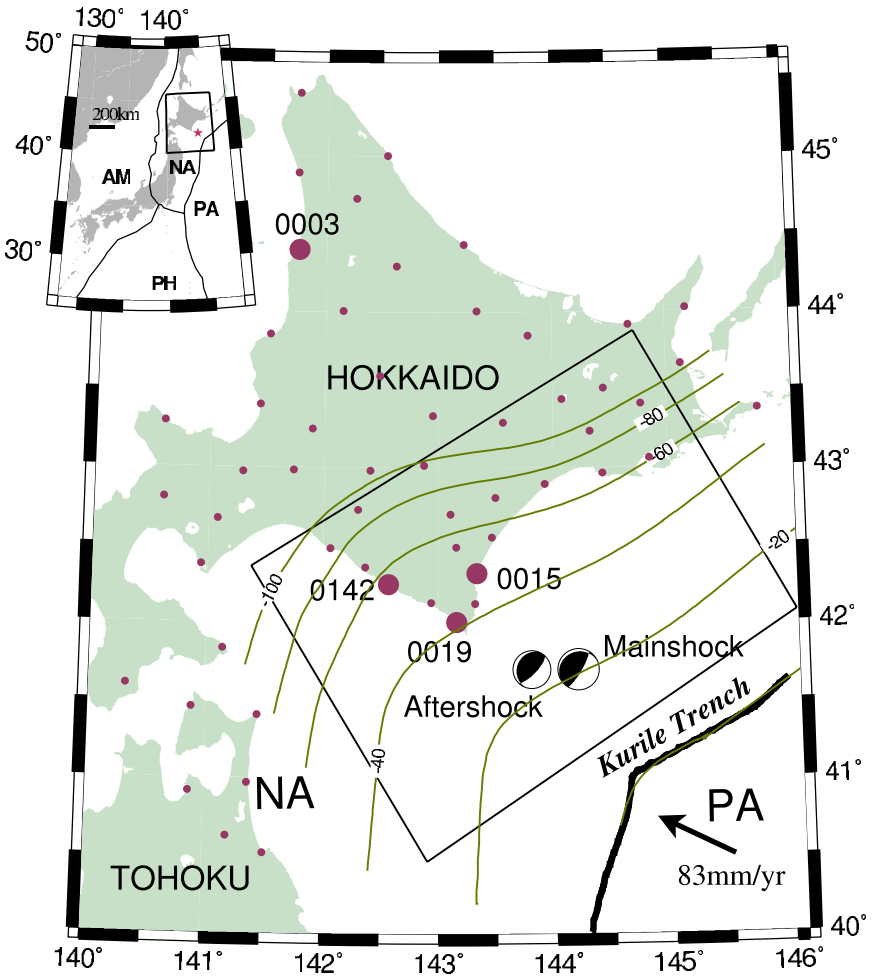

Figure 1. GEONET stations used in this study are shown with circles; large numbered circles correspond to stations shown in Figure 2. Inset shows location of the GPS network with respect to the global tectonic framework. Epicenters of the 2003 Tokachi-oki earthquake mainshock and the largest aftershock are shown with mechanisms taken from NIED F-NET solution (http://www.fnet.bosai.go.jp/freesia/index.html). The depth of the plate interface is contoured in kilometers. The fault plane used in the inversion is outlined in black.

Tokachi-oki mainshock, there were telemetry-related 1-Hz outages at most of the sites closest to the epicenter. In order to be consistent, only the 30-second GPS data are used in this study. These data had no significant outages during the earthquakes and the early postseismic period. Data from a total of 55 GEONET stations shown in Figure 1 were analyzed using the GIPSY software [*Lichten and Borders*, 1987] and the ITRF2000 reference frame [*Altamimi et al.*, 2002]. Estimates for coseismic and postseismic deformation are derived in the following manner. Positions of three IGS sites in Russia, Japan, and China (YAKT, USUD and WUHN), IGS orbits and Earth orientation are held fixed. The positions for the GEONET sites are estimated every 30 seconds, along with carrier phase ambiguities, random-walk constrained troposphere zenith delays, and transmitter/receiver clocks. In order to estimate coseismic steps for the mainshock and aftershock, GIPSY was modified to allow white noise resets at the times of the earthquakes, with positions modeled as a tightly constrained random walk process at other times to reduce multipath (K. M. Larson, Resolving static offsets from high-rate GPS Data: The 2003 Tokachi-oki Earthquake, submitted to Earth, Planets, Space, 2007, available online http://xenon.colorado.edu/larson_eps_2007.pdf) (hereinafter referred to as Larson, submitted manuscript, 2007). For postseismic analysis, no constraints are put on the GEONET position estimates. Although this strategy results in the presence of significant common-mode errors in the GPS time series, the subsequent inversion can be used to solve for these terms simultaneously with fault slip. This latter strategy was adopted to avoid double temporal smoothing by GIPSY and the Network Inversion Filter [*Segall and Matthews*, 1997]. Examples of GPS time series showing postseismic slip are shown in Figure 2. Note that coseismic displacements and common mode errors have already been removed.

[8] The coseismic steps estimated by Larson (submitted manuscript, 2007) have been inverted to infer slip distributions for the mainshock and the largest aftershock. Smoothing and minimum norm constraints are imposed on the inversion. The same fault geometry as *Miyazaki et al.* [2004a] is adopted, but regions from both the mainshock and afterslip where no significant slip was found are deleted to loosen the penalty term for slip. The model region used is 320 km in length and 246 km in width. Its northeastern edge

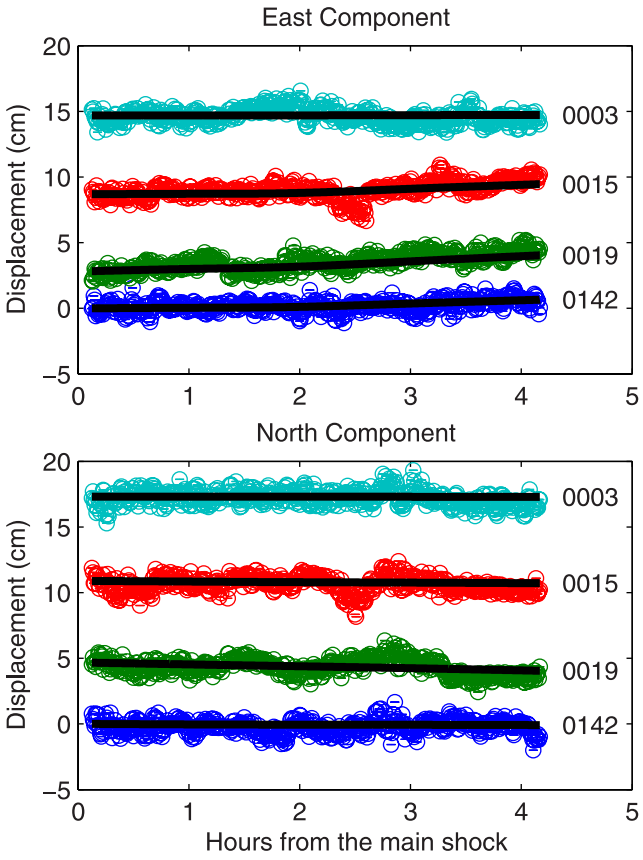

Figure 2. Horizontal GPS time series at selected stations: 0003, 0015, 0019, and 0142. Time zero corresponds to the time of the mainshock. The largest aftershock occurred at t = 1.3 (*hr*). Thirty second solutions are shown with open circles. The solid line shows the modeled fault slip prediction, excluding random benchmark motion. Common-mode noise has been subtracted from both observed and predicted data.

is located at 144.7°E, 43.9°N, and it is subdivided it into 13 × 11 segments (see Figure 1). Slip is expanded in two-dimensional B-spline functions of order 3 following *Yabuki and Matsu'ura* [1992]. The relative weight of spatial smoothing and minimum norm constraints are determined by minimizing ABIC [*Akaike*, 1980].

[9] The 30-second position estimates from 9/25 19:57:30 to 9/26 00:00:00 are inverted to infer the space-time evolution of the fault slip after the mainshock using the Network Inversion Filter with the same fault geometry as coseismic inversions. Hyperparameters for the temporal and spatial smoothing and minimum norm constraint are optimized by minimizing ABIC, instead of using the Extended Network Inversion Filter (ENIF) [*McGuire and Segall*, 2003], because hyperparameter estimation by ENIF is sensitive to its *a priori* value. Tight constraints are imposed for the benchmark wobble term to suppress trade-offs with fault slip.

4. Results

[10] Estimated coseismic slip for the mainshock is shown in Figure 3a. The slip is downdip of the epicenter with a maximum amplitude of ~5.3 m (at 144°E, 42°N), with typical slip uncertainties of about 0.7 m and 1.5 m at the deepest and the shallowest part of the fault. Although backward slip is inferred, it is within the uncertainties. The normalized RMS is 1.11. Slip is not well resolved in the shallower (<15 km depth) part of the fault, however the major part of coseismic slip is found in the resolvable region. (see the auxiliary material[1] for further information on model fit and resolution.)

[11] This study gives the first geodetic estimation of the coseismic slip for the M7.4 aftershock (Figure 3b). Because it is much smaller, occurred soon after the mainshock, and would be obscured by 24-hour position averages, it has been more difficult to study this earthquake. The inferred slip is just a few tens of km west of its epicenter with maximum amplitude of about 30 cm (at 143.5°E, 41.6°N). Typical uncertainties for slip are 6 cm and 10 cm at the deepest and shallowest part of the fault, with similar resolution regions as in the inversion for the mainshock. The normalized RMS is 1.07.

[12] Afterslip is observed immediately after the mainshock. The cumulative afterslip for the period between the mainshock and the largest aftershock (period 1: Sep.25 19:57:30 ~21:08:00) is shown in Figure 3c. In order to prevent the slip after the second earthquake from smearing into period 1, only forward filtered slip estimates are used. In other words, slip shown in Figure 3c is estimated from data only between the two earthquakes. Maximum slip of ~3.4 cm is found between two coseismic slip loci. Again the majority of slip is found in resolvable regions, with typical uncertainties of 0.6–0.7 cm. The cumulative slip for the entire time series (period 2: Sep.25 19:57:30 ~ Sep.26 00:00:00) is shown in Figure 3d. Similar to the slip during period 1, the slip locus with a maximum amplitude of about 7.3 cm is found in the region between the two epicenters, a slightly shallower part than the coseismic slip loci. In addition, a larger slip locus with the maximum amplitude of about 11.6 cm is found in the downdip extension of the afterslip. The typical uncertainties for the slip are 1.0–1.2 cm.

[13] The sequence of slip history suggests that the mainshock triggered afterslip just to the southwest of its rupture region, which then triggered the M7.4 aftershock in the farther southwest region. More afterslip was triggered by the second earthquake (or possibly by the combined effect of the two earthquakes) at the downdip extension of the two earthquakes. The initial afterslip locus continued to slip after the second earthquake, but it appears that the slip also propagated slightly updip in spite of the limited resolution in the updip. Although the inferred slip distribution tends to be spread out due to spatial smoothing constraints imposed in our inversions, two afterslip loci are inferred outside the main rupture regions. This could be a manifestation that the frictional properties on the plate interface at the Kurile Trench are non-uniform, as suggested by *Miyazaki et al.* [2004a] and *Baba et al.* [2006].

5. Discussion

[14] The inversion results suggest that the speed of afterslip propagation is non-uniform in the dip direction; updip

[1] Auxiliary materials are available in the HTML. doi:10.1029/2007GL032309.

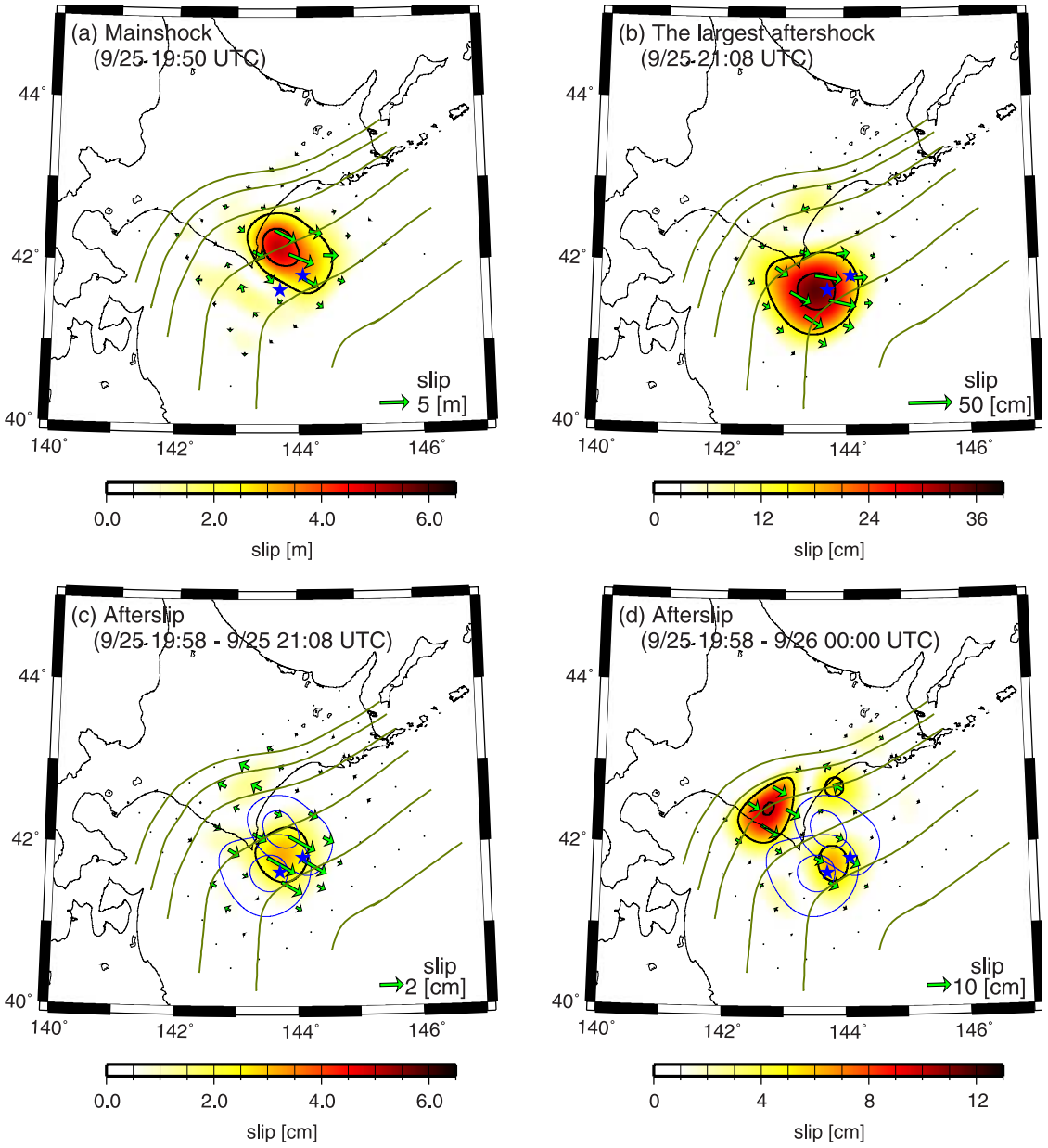

Figure 3. Coseismic slip distribution for (a) the 2003 Tokachi-oki earthquake, (b) the largest aftershock, (c) cumulative afterslip during the period between those two earthquakes, and (d) cumulative afterslip between the mainshock and Sept.26 00:00. The two asterisks represent epicenters for those two earthquakes. Contour intervals for slip for Figures 3a, 3b, 3c, and 3d are 2 m, 15 cm, 2 cm, 5 cm, respectively.

afterslip propagates faster and afterslip downdip propagation is significantly slower than updip slip. What causes the differences in the afterslip propagation speed?

[15] *Ariyoshi et al.* [2007] conducted a numerical simulation study with a two-dimensional planar fault based on rate- and state-dependent friction laws [*Dietrich*, 1979]. Their model contains one velocity weakening patch ("asperity") which is surrounded by a velocity strengthening zone. For several simulation results, they found that the depth-dependence of the effective normal stress σ_{eff} (i.e. normal stress minus pore pressure) causes slow afterslip propagation in the downdip part and faster afterslip propagation in the shallow updip portion of the fault. *Ariyoshi et al.* [2007] investigated small repeating earthquakes following the 1994 Sanriku Haruka-oki earthquake ($M_w \sim 7.4$) to obtain averaged cumulative afterslip histories, and found them to be consistent with their own simulation results.

[16] Another possible model for non-uniform afterslip propagation speed is proposed by *Kato* [2004]. This model involves two equal-sized velocity weakening patches, with one having more unstable frictional properties, surrounded by velocity-strengthening zones. He showed that afterslip follows an earthquake at one weakening patch and the second patch starts to rupture when the afterslip reaches it. He also showed that the afterslip propagates faster as the distance between the two asperities becomes smaller. In the case of the 2003 Tokachi-oki earthquake, the closest weakening patches in the trench-parallel direction are the largest

aftershock (Figure 3b) to southwest and possibly the 1973 Nemuro-oki earthquake to the northeast. Since the distance to the largest aftershock area is shorter, afterslip may have propagated faster to southwest. One possible interpretation for this effect is that the velocity strengthening zone between two weakening zones is partially locked during the interseismic period because weakening zones of both edges are strongly locked and prevent the strengthening zone from freely slipping with the plate velocity.

[17] *Miyazaki et al.* [2004a] estimated afterslip for 30 days and found significant slip in regions at similar depth to the mainshock rupture region, where no significant slip is inferred from four hours of GPS data. This difference would imply that the afterslip in these regions accelerated more slowly than updip-downdip regions.

[18] Following *Miyazaki et al.* [2004a], we calculated shear stress changes at the afterslip regions. The shear stress decreased while the sliprates are nearly constant. Because we did not use the first few minutes of GPS data following the mainshock, we may have missed the acceleration phase. The transition time scale from dynamic to static may help constrain the frictional properties of faults.

6. Conclusions

[19] The early phases of afterslip following the 2003 Tokachi-oki earthquake have been investigated. GPS station positions estimated every 30 seconds are used to invert for the space-time evolution of afterslip. Coseismic slip for the mainshock and its largest aftershock are also modeled. The afterslip that occurs between the two earthquakes is located between the two epicentral areas. Subsequently a deeper part of the fault started to slip. Less significant slip was inferred in the eastern side of the mainshock region, where significant afterslip was previously found for periods of one month to a year. The trench perpendicular and parallel non-uniformities of the afterslip propagation may be described by depth-dependence of the effective normal stress and distance between two velocity weakening patches, respectively. This analysis demonstrates how subdaily GPS can provide additional constraints on fault frictional properties for studies of megathrust earthquakes, particularly when GPS networks are built in plate boundary zones.

[20] **Acknowledgments.** S.M. acknowledges JSPS grant 17740286. K.L. acknowledges the support of NSF EAR-0538116, a JSPS travel fellowship, and Kyuhong Choi. Review comments by Jessica Murray and Mohamed Chlieh significantly improved the manuscript. Discussions with Takane Hori, Naoyuki Kato, Paul Segall, Kaj Johnson and Junichi Fukuda were useful. We are grateful to GSI for providing the GPS data.

References

Akaike, H. (1980) Likelihood and the Bayes procedure, in Bayesian Statistics, edited by J. M. Bernardo et al., pp. 141–166, Univ. Press, Valencia, Spain.

Altamimi, Z., P. Sillard, and C. Boucher (2002), ITRF2000: A new release of the International Terrestrial Reference Frame for earth science applications, *J. Geophys. Res.*, *107*(B10), 2214, doi:10.1029/2001JB000561.

Ariyoshi, K., T. Matsuzawa, and A. Hasegawa (2007), The key frictional parameters controlling spatial variations in the speed of postseismic-slip propagation on a subduction plate boundary, *Earth Planet. Sci. Lett.*, *256*, 136–146.

Baba, T., K. Hirata, T. Hori, and H. Sakaguchi (2006), Offshore geodetic data conducive to the estimation of the afterslip distribution following the 2003 Tokachi-oki earthquake, *Earth Planet Sci. Lett.*, *241*, 281–292.

Dietrich, J. H. (1979), Modeling of rock friction:1. Experimental results and constitutive equations, *J. Geophys. Res.*, *84*, 2161–2168.

Freymueller, J., N. E. King, and P. Segall (1994), The co-seismic slip distribution of the Landers earthquake, *Bull. Seismol. Soc. Am.*, *84*(3), 646–659.

Heki, K., S. Miyazaki, and H. Tsuji (1997), Silent fault slip following an interplate thrust earthquake at the Japan Trench, *Nature*, *386*, 595–597.

Hirose, H., and K. Hirahara (2004), A 3-D quasi-static model for a variety of slip behaviors on a subduction fault, *Pure Appl. Geophys.*, *161*, 2417–2431.

Honda, R., S. Aoi, N. Morikawa, H. Sekiguchi, T. Knugi, and H. Fujiwara (2004), Ground motion and rupture process of the 2003 Tokachi-oki earthquake obtained from strong motion data of K-net and KiK-net, *Earth Planets Space*, *56*, 317–322.

Ji, C., K. M. Larson, Y. Tan, K. Hudnut, and K. Choi (2004), Slip history of the 2003 San Simeon Earthquake constrained by combining 1-Hz GPS, strong motion, and teleseismic data, *Geophys. Res. Lett.*, *31*, L17608, doi:10.1029/2004GL020448.

Johnson, K. M., Y. Hsu, P. Segall, and S. Yu (2001), Fault geometry and slip distribution of the 1999 Chi-Chi, Taiwan earthquake imaged from inversion of GPS data, *Geophys. Res. Lett.*, *28*(11), 2285–2288.

Kato, N. (2004), Interaction of slip on asperities: Numerical simulation of seismic cycles on a two-dimensional planar fault with nonuniform frictional property, *J. Geophys. Res.*, *109*, B12306, doi:10.1029/2004JB003001.

Kawasaki, I., Y. Asai, Y. Tamura, T. Sagiya, N. Mikami, Y. Okada, M. Sakata, and M. Kasahara (1995), The 1992 Sanriku-Oki, Japan, ultra-slow earthquake, *J. Phys. Earth.*, *43*, 105–116.

Koketsu, K., K. Hikima, S. Miyazaki, and S. Ide (2004), Joint inversion of strong motion and geodetic data for the source process of the 2003 Tokachi-oki, Hokkaido, earthquake, *Earth Planets Space*, *56*, 329–334.

Lichten, S., and J. Borders (1987), Strategies for high-precision global positioning system orbit determination, *J. Geophys. Res.*, *92*, 12,751–12,762.

Ma, K., J. Mori, S. Lee, and S. B. Yu (2001), Spatial and temporal distribution of slip for the 1999 Chi-Chi, *Taiwan, earthquake, Bull. Seismol. Soc. Am.*, *91*(5), 1069–1087.

McGuire, J. J., and P. Segall (2003), Imaging of aseismic slip transients recorded by dense geodetic networks, *Geophys. J. Int.*, *155*, 778–788.

Miura, S., Y. Suwa, A. Hasegawa, and T. Nishimura (2004), The 2003 M8.0 Tokachi-Oki earthquake: How much has the great event paid back slip debts?, *Geophys. Res. Lett.*, *31*, L05613, doi:10.1029/2003GL019021.

Miyazaki, S., P. Segall, J. Fukuda, and T. Kato (2004a), Space time distribution of afterslip following the 2003 Tokachi-oki earthquake: Implications for variations in fault zone frictional properties, *Geophys. Res. Lett.*, *31*, L06623, doi:10.1029/2003GL019410.

Miyazaki, S., K. Larson, K. Choi, K. Hikima, K. Koketsu, P. Bodin, J. Haase, G. Emore, and A. Yamagiwa (2004b), Modeling the rupture process of the 2003 Tokachi-Oki earthquake using 1-Hz GPS data, *Geophys. Res. Lett.*, *31*, L21603, doi:10.1029/2004GL021457.

Ozawa, S., M. Kaidzu, M. Murakami, T. Imakiire, and Y. Hatanaka (2004), Coseismic and postseismic crustal deformation after the M_w 8 Tokachi-oki earthquake in Japan, *Earth Planets Space*, *56*, 675–680.

Segall, P., and M. Matthews (1997), Time-dependent inversion of geodetic data, *J. Geophys. Res.*, *102*, 22,391–22,410.

Tanaka, Y. (2007), Modeling viscoelastic postseismic deformation, *J. Geodyn. Soc. Jpn.*, *53*, 35–50.

Yabuki, T., and M. Matsu'ura (1992), Geodetic data inversion using a Bayesian information criterion for spatial distribution of fault slip, *Geophys. J. Int.*, *109*, 363–375.

Yagi, Y. (2004), Source rupture process of the 2003 Tokachi-oki earthquake determined by joint inversion of teleseismic body wave and strong ground motion data, *Earth Planets Space*, *56*, 311–316.

Yamanaka, Y., and M. Kikuchi (2003), Source processes of the recurrent Tokachi-oki earthquake on September 26, 2003, inferred from teleseismic body waves, *Earth Planets. Space*, *55*, e21–e24.

K. M. Larson, Department of Aerospace Engineering Sciences, University of Colorado, Boulder, CO 80309-0429, USA. (kristinem.larson@gmail.com)

S. Miyazaki, Earthquake Research Institute, University of Tokyo, Tokyo, 113-0032, Japan. (miyazaki@eri.u-tokyo.ac.jp)